JOURNAL OF MATERIALS SCIENCE 17 (1982) 3021–3038

The calculated defect structure of bulk and {001} surface cation dopants in MgO

E. A. COLBOURN, W. C. MACKRODT
ICI PLC, New Science Group, The Heath, Runcorn, Cheshire, UK

Lattice defect calculations are presented for the cation doping of the bulk and {001} surface of MgO by Li^+, Na^+, Be^{2+}, Ca^{2+}, Fe^{2+}, Al^{3+}, Sc^{3+}, Fe^{3+}, Ti^{4+} and Si^{4+}. Interionic potentials are derived from electron-gas calculations while the lattice relaxation methods are essentially those introduced by Lidiard and Norgett. An emphasis is placed on the differences between the bulk and surface, and, where possible, a comparison is made with the available experimental data.

1. Introduction

In view of its importance both in fundamental research in ceramics and in areas of application such as heterogeneous catalysis, the defect structure of magnesium oxide has been the subject of extensive study for a number of years. Central to this study is the role played by cation impurities, a number of which are present in the purest materials and are largely responsible, therefore, for many of its electrical [1, 2], optical [3], mass-transport [4, 5], and reactive properties [6, 7]. While experiment continues to be the major source of information about this, as indeed about other refractory oxides, recent advances in theoretical methods and computational procedures [8–11] suggest that calculations might make a significant contribution to our knowledge of the defect structure, especially in circumstances in which either the appropriate experiments are difficult to perform accurately, or the results open to ambiguous interpretation.

It now seems probable that intrinsic defects in MgO are present only at the highest temperatures and even then in extremely low concentrations. For the most part lattice disorder is governed by the level and nature of the impurities, although the precise details of this disorder remain uncertain for the majority of cations as Gourdin and Kingery have pointed out recently [12]. Trivalent impurites such as Al^{3+}, Sc^{3+}, Cr^{3+} and Fe^{3+} have received most attention, at least in the bulk, and are thought to give rise to magnesium vacancies; while in a few cases impurity–vacancy association energies have been reported [4, 12, 13]. Information about other cations, however, whether isovalent such as Be^{2+}, Ca^{2+} and Fe^{2+}, or aliovalent such as Li^+, Na^+, Si^{4+} and Ti^{4+}, remains sparse, except for the alkali ion V-centres [14–16].

A further problem associated with impurity defects relates to possible differences between the crystal bulk and interfaces such as surfaces and grain boundaries [17, 18]. Recent experiments have indicated that Ca^{2+}, Al^{3+}, Sc^{3+}, Fe^{3+}, La^{3+}, Si^{4+} and Ti^{4+} segregate at grain boundaries [19–21], while Black and Kingery [22] have reported that Sc^{3+}, Cr^{3+} and Fe^{3+}, but not Fe^{2+} segregate at the {001} surface. Ca^{2+} [23] and Zn^{2+} [24] also appear to concentrate at the surface as does Al^{3+}; but in the case of the latter it seems to be accompanied by spinel formation [25, 26].

In view of this situation, then, it would seem worthwhile giving a *unified theoretical description* of both the bulk and surface defect structure of MgO induced by a variety of mono-, di-, tri- and quadrivalent cations with three purposes in mind. The first is to compare the predicted bulk and surface defect energies, for comparisons of this sort appear to be rather limited at present [27, 28]. The second is to assess the accuracy of these calculations in relation to such data as exists, particularly for surfaces [22–26]. Finally it is our purpose to stimulate further experiment in those areas where theoretical information is available or can be easily obtained but where the data are either limited or non-existent. Accord-

0022–2461/82/103021–18$04.66/0

ingly, in this paper we present calculations of the defect structure of MgO doped with Li^+, Na^+, Be^{2+}, Ca^{2+}, Fe^{2+}, Al^{3+}, Sc^{3+}, Fe^{3+}, Si^{4+} and Ti^{4+} both in the bulk and at the {0 0 1} surface and compare the results with what can be deduced reliably from experiment. Calculations for some of the bulk defects considered have been reported previously [29, 30], although in the majority of cases this is not so, while those for the surfaces are presented here for the first time.

Our emphasis on the term "unified theoretical description" is intended to stress two important aspects of defect calculations of the type reported here. The first is that in many instances differences between bulk and surface energies are small so that it is essential that the treatment of lattice relaxation is as near identical as possible in both cases. As on previous occasions [27–30] the procedures used in the present calculations ensure that this is so. The second point is that a comparison of impurity effects, if it is to be consistent, requires the use of consistent theoretical methods and in particular those used to derive interatomic potentials; for the latter ultimately determine the nature of the defect structures and the magnitude of the energies involved. All our calculations, therefore, are based on a *single* procedure for determining interatomic potentials, namely the modified electron-gas approximation discussed recently in some detail [29]. Despite its limitations [31], this is the only theoretical procedure available that (a) calculates impurity potentials which are consistent with the host lattice, that is to say, they are calculated at the same level of approximation, (b) distinguishes between different host lattices with regard to impurity potentials, and (c) calculates potentials for different charged states in a completely equivalent way.

The outline of this paper, then, is as follows. In Section 2 we summarize the methods used for deriving interatomic potentials and the determination of lattice relaxation, while in Section 3 we present our detailed calculations of the defect structure associated with cation impurities.

2. Theory of lattice defect calculations

For materials such as MgO that are ionic, or nearly so, the theory of lattice defect calculations is largely concerned with two principal problems. They are the evaluation of interatomic potentials and the treatment of lattice relaxation. Both have been reviewed recently in some detail [11, 32], so that only those features that are relevant to the present calculations will be discussed and even then only briefly.

2.1. Interatomic potentials

Here, as elsewhere [27–30], interatomic potentials are assumed to be exclusively two-body in nature, with an explicit allowance for electronic polarization of the lattice by means of the shell-model proposed by Dick and Overhauser [33]. The non-polarizable contribution to the total potential, $E(R)$ is calculated on the basis of a modified electron-gas approximation [29, 34–37]. It includes the self-energy correction suggested by Rae [38] and is given by

$$E(R) = \frac{Z_A Z_B}{R} - Z_B \int \frac{\rho_A(r_1)}{r_{1B}} dr_1 - Z_A \int \frac{\rho_A(r_2)}{r_{2A}} dr_2 + \int\int \frac{\rho_A(r_1)\rho_B(r_2)}{r_{12}} dr_1\, dr_2 + \int \{[\rho_A(r) + \rho_B(r)]\, E_G[\rho_A(r) + \rho_B(r)] - \rho_A(r) \times E_G[\rho_A(r)] - \rho_B(r) E_G[\rho_B(r)]\}\, dr \quad (1)$$

in which

$$E_G[\rho(r)] = C_K[\rho(r)]^{2/3} + C_e[1 - 8/3\delta + 2\delta^2 + 1/3\delta^4]\,[\rho(r)]^{1/3} + \epsilon_c[\rho(r)]. \quad (2)$$

In Equations 1 and 2 Z_A and Z_B are the nuclear charges of the ions, $\rho_A(r)$ and $\rho_B(r)$ their respective electron densities, and ϵ_C the correlation energy density derived by Gordon and Kim [34]. The factors C_k and C_e are given by

$$C_k = (3/10)(3\pi^2)^{2/3} \text{ and } C_e = (3/4)(3/\pi)^{1/3}$$

while δ is determined [38] from the equation,

$$(4N)^{-1} = \delta^3 (1 - 9/8\delta + 1/4\delta^3), \quad (3)$$

where N is the total number of electrons of the two ions. Cation densities are taken as the free-ion values whereas the oxygen density is obtained from single-centre Hartree–Fock calculations with an effective potential that simulates the Madelung field of the crystal [29].

Full numerical details of all the potentials used in the present calculations are given in a recent compilation of Colbourn *et al.* [39], so that here we simply illustrate the variations in the non-coulombic contributions to impurity–host lattice interactions. These are shown in Figs. 1 to 4. While

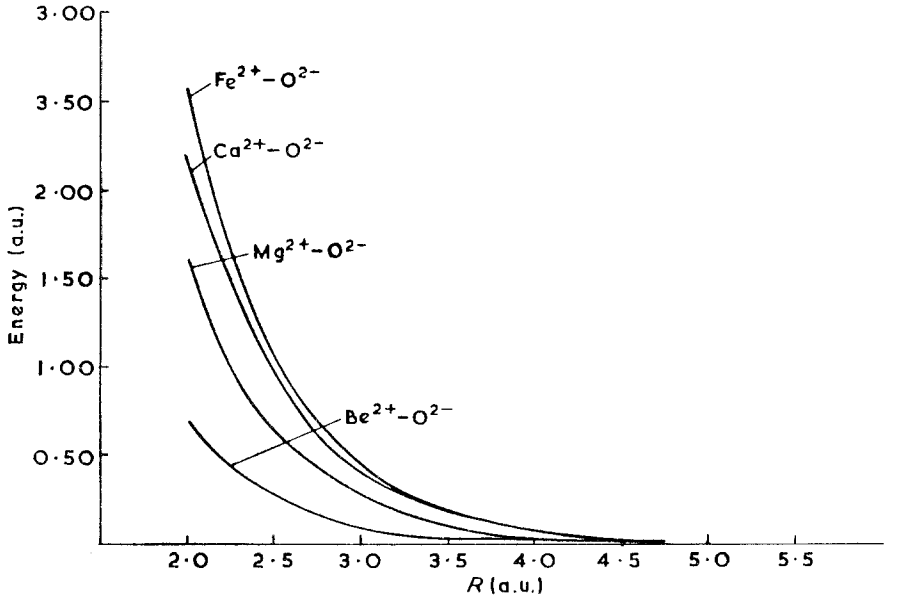

Figure 1 Non-coulombic potentials for monovalent ions.

it is true that for the most part these variations reflect in a straightforward way differences in ion size, the important point is that they are calculated in a consistent way for the entire range of impurities examined here.

2.2. Lattice relaxation

The treatment of lattice relaxation used in the present calculations is essentially that developed by Lidiard and Norgett [8] and Norgett [9, 10] and modified for sufaces by Mackrodt and Stewart [28]. The general formulation is based on the notion that the total energy of the system is minimized by a relaxation of the ions surrounding a defect and that this relaxation decreases fairly rapidly for distances away from the defect. As a result, the crystal can be formally partitioned into an inner region I, in which the lattice configuration is evaluated explicitly, and an outer region II, which as far as the defect is concerned can be viewed as a quasi-continuum, within which the displacements can be calculated on the basis of some suitable approximation.

The total energy of the system is written as

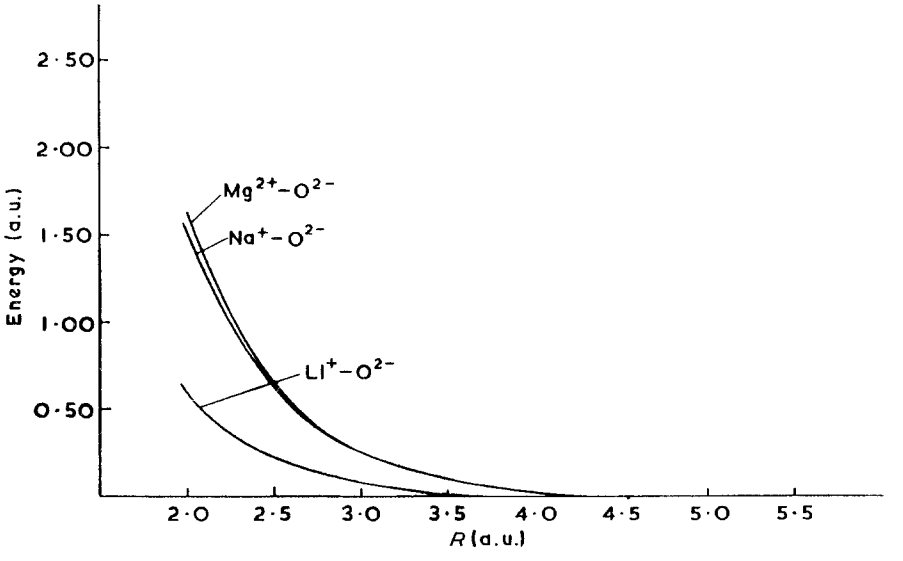

Figure 2 Non-coulombic potentials for divalent ions.

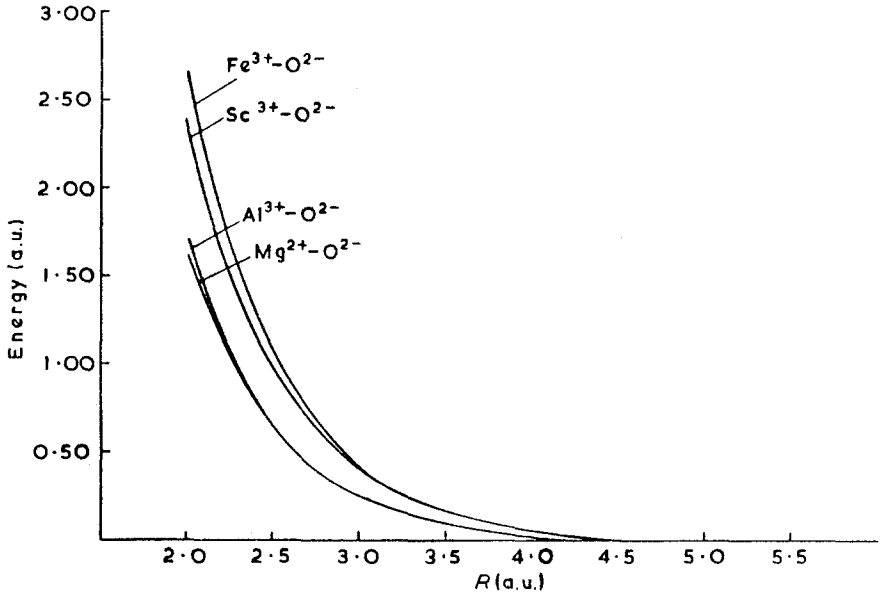

Figure 3 Non-coulombic potentials for trivalent ions.

$$E = E_{\mathrm{I}}(\mathbf{X}) + E_{\mathrm{II}}(\mathbf{Y}) + E_{\mathrm{I,II}}(\mathbf{X},\mathbf{Y}), \qquad (4)$$

in which $E_{\mathrm{I}}(\mathbf{X})$ is the energy of the inner region, $E_{\mathrm{II}}(\mathbf{Y})$, the energy of the outer region and $E_{\mathrm{I,II}}(\mathbf{X}, \mathbf{Y})$, the interaction energy between regions I and II. **X** is a vector of the independent displacements of ions in the inner region, while **Y** is the corresponding vector for the outer region. The components of **X** are determined by solving the appropriate "force-balance" equations which result from the requirement that the force on each ion in region I is zero. The components of **Y**, on the other hand, are derived on the basis of the Mott–Littleton approximation. A detailed account of these procedures is given in [11].

3. Defect calculations

The theoretical methods outlined briefly above were used to calculate lattice defect energies associated with Li^+, Na^+, Be^{2+}, Ca^{2+}, Fe^{2+}, Al^{3+}, Sc^{3+}, Fe^{3+}, Ti^{4+}, and Si^{4+} in MgO, both in the bulk and at the {0 0 1} surface. In all the calcu-

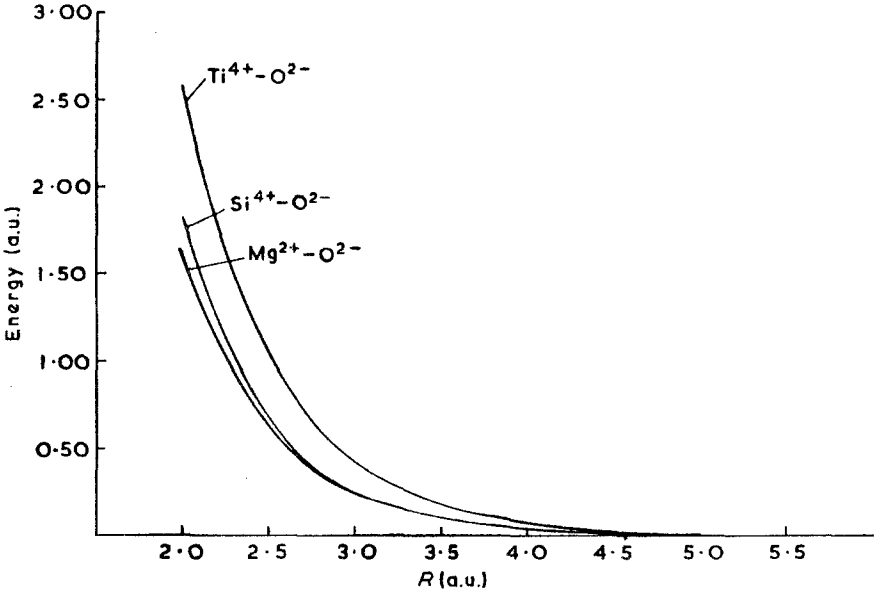

Figure 4 Non-coulombic potentials for quadivalent ions.

lations reported here, except those for the impurity–vacancy dimer at the surface, more than a hundred ions were relaxed explicitly in the inner region. This ensured an energy convergence to less than 0.001 eV. For dimeric impurity associates at the surface, however, the lower symmetry of the system reduces the size of the inner region that can be dealt with at present. Up to fifty ions could be explicitly relaxed and the corresponding defect energies fitted to a simple function of the region size. From this, the extrapolated energies for infinite region I could be obtained with an estimated error of less than 0.05 eV in all cases. As on previous occasions [27, 28] defect energies at the {001} surface refer to the fully relaxed surface, that is to say, surfaces at which both cores and shells have reached their equilibrium positions. Our complete set of results is given collectively in Tables II to XIII, while for convenience the fundamental defect energies are summarized in Table I. We now consider the individual impurities in detail.

3.1. Li^+

In the absence of oxygen exchange, Li^+ substitution can be compensated by either anion vacancies or cation interstitials. At the high-temperature limit, or alternatively at infinite dilution, that is to say when no association is allowed for, the calculated heats of solution per Li^+_{Mg} ion are 2.78 and 4.90 eV, respectively, which suggests that vacancy compensation is the more favourable of the two models by far. The {100} dimer, $(Li^+_{Mg}–V_O)$ is bound by 1.42 eV with respect to the isolated defects, while the interaction energy of the corresponding trimer, $(Li^+_{Mg}–V_O–Li^+_{Mg})$, is −2.74 eV, or −1.37 eV per Li^+_{Mg}. This reduces the calculated heat of solution to approximately 1.4 eV. Free interstitial Li^+_I and its associated defects, namely cation vacancies and anion interstitials, are found to be highly energetic; however, as before this is drastically reduced by association. In particular, the trimer, $(Li^+_I–V_{Mg}–Li^+_I)$, in which two lithium ions and a cation vacancy form a linear complex in the {111} direction, is bound by more than 8 eV with respect to the isolated defects. We predict it to be the lowest energy neutral defect in MgO, with a heat of solution of 0.72 eV. However, the energy difference between this and the anion vacancy trimer, $(Li^+_{Mg}–V_O–Li^+_{Mg})$ is small, suggesting that both are likely to exist. The calculated enthalpy change for the equilibrium,

$$(Li^+_{Mg}–V_O–Li^+_{Mg}) + MgO \rightarrow (Li^+_I–V_{Mg}–Li^+_I)$$

is −1.37 eV. Our calculations suggest, therefore, that Li_2O should have an appreciable solubility in MgO, by either mode of solution. The interstitial trimer $(Li^+_I–V_{Mg}–Li^+_I)$ is similar to that proposed by Kim and Nowick [40] for Li^+ impurities in MgF_2 and subsequently confirmed theoretically by Catlow and James [41]. It is also similar to the {111} complex $(O^-_I–V_O–O^-_I)$ in alkaline-earth oxides discussed by Mackrodt and Stewart [30]. The barrier for rotation through the {110} direction is calculated to be 0.46 eV which is similar to both the theoretical value of 0.66 eV and the experimental value of 0.42 eV for Li^+ in MgF_2 [40]. We suggest, therefore, that dielectric relaxation of the same type should occur for Li^+ in MgO.

The reduced symmetry that surfaces inevitably impose limits the range of defects for which calculations comparable in accuracy to the bulk can be performed. For Li^+ at the {001} surface, therefore, we have not been able to include interstitial defects in the present report and confine our attention to the isolated substitution, Li^+_{Mg}, and the neutral vacancy trimer. The differences between the bulk and surface follow the trend previously found for Li^+ in NaF [28], namely that Li^+_{Mg} is predicted to be marginally more stable in the bulk, whereas the neutral trimer is lower in energy by approximately 1.2 eV at the {001} surface. Now in general these differences are governed by three factors, namely, the Madelung potential, the (electronic) polarization of the lattice and its

TABLE I Fundamental energies for MgO. Lattice energy = −40.75 eV

	(eV)	
(a) Bulk defects		
Formation energy of:		
cation vacancy	25.41	(23.83)*
anion vacancy	22.91	(24.70)
cation (Mg^{2+}) interstitial	−13.59	(−12.41)
anion (O^{2-}) interstitial	−7.74	(−12.60)
Schottky pair	7.57	(7.7)
(b) {001} surface defects		
Formation energy of:		
cation vacancy	25.91	
anion vacancy	23.33	

*Figures in brackets are the corresponding defect energies based on the potential derived by Catlow *et al.* [50] and used by Gourdin and Kingery [12].

elastic deformation. In the case of Li^{+}_{Mg}, both the electrostatic and elastic energy contributions favour the surface, whereas the polarization energy, due largely to long-range charge-induced dipoles, is greater in the bulk. As shown in Table II, the overall energy is slightly lower in the bulk. The relative stability of the trimer (Li^{+}_{Mg}–V_O–Li^{+}_{Mg}), on the other hand, as with all neutral defects, is determined solely by the local elastic deformation, including short-range polarization effects. Here it is predicted to favour the surface. At equilibrium, therefore, the present calculations suggest a surface enrichment by Li^+, although this view might require modification once interstitial defects can be taken into account.

As we have indicated, the present calculations specifically refer to conditions under which there is no exchange of oxygen, a situation for which there seems to be no experimental data. Defect calculations involving the oxidation and reduction of MgO will be reported separately [42], when we will be able to make direct comparison with experiment [14–16].

3.2. Na^+

The doping of MgO by Na^+ is both interesting in itself and in relation to Li^+, for the two are distinguished largely by the difference in ionic radius and hence by the elastic response of the lattice. Thus, the energy for the isolated defect is increased from 16.27 eV for Li^{+}_{Mg} to 18.64 eV for Na^{+}_{Mg}. However, the lower lattice energy of Na_2O, −27.10 eV compared with −31.60 eV for Li_2O, leads to heats of solution for free vacancy and interstitial compensation which are very similar for the two monovalent oxides. The binding energies of both the {100} dimer and trimer are within 0.1 eV of the corresponding Li^+ defects,

TABLE II Doping of MgO by Li^+. Lattice energy of Li_2O = −31.60 eV*

	(eV)
(a) Bulk defects	
(i) *Li^+ substitution*	
Defect energy of Li^{+}_{Mg}	16.27
Calculated heat of solution *per Li^+ ion*:	
Free anion vacancy compensation	2.78
Free cation interstitial compensation	4.90
Defect energy of {100} (Li^{+}_{Mg}–V_O) complex	37.76
Interaction energy of free Li^{+}_{Mg} and V_O (anion vacancy)	−1.42
Defect energy of {100} (Li^{+}_{Mg}–V_O–Li^{+}_{Mg}) complex	52.71
Interaction energy of Li^{+}_{Mg} and (Li^{+}_{Mg}–V_O)	−1.32
Total interaction energy of two Li^{+}_{Mg} and V_O	−2.74
Calculated heat of solution per Li^+ ion	1.41
(ii) *Li^+ interstitial*	
Defect energy of Li^{+}_{I}	−3.22
Calculated heat of solution per Li^+ ion	
Free cation vacancy compensation	4.91
Free anion interstitial compensation	8.71
Defect energy of {111} (Li^{+}_{I}–V_{Mg}–Li^{+}_{I}) complex	10.59
Total interaction energy of two Li^{+}_{I} and V_{Mg}	−8.38
Calculated heat of solution per Li^+ ion	0.72
Defect energy of {110} (Li^{+}_{I}–V_{Mg}–Li^{+}_{I}) complex	11.05
Rotation barrier of (Li^{+}_{I}–V_{Mg}–Li^{+}_{I}) complex thrqugh {110} direction	0.46
Defect energy of $\{\frac{1}{2}00\}$ (Li^{+}_{I}–O^{2-}_{I}–Li^{+}_{I}) complex	−18.34
Total interaction energy of two Li^{+}_{I} and O^{2-}_{I}	−4.16
Calculated heat of solution per Li^+ ion	6.46
Activation energy for Li^+ interstitial migration	0.97
(b) {001} surface defects	
Defect energy of Li^{+}_{Mg}	16.40
Defect energy of (Li^{+}_{Mg}–V_O–Li^{+}_{Mg})	51.52
Total interaction energy of two Li^{+}_{Mg} and V_O *in the* {001} *surface plane*	−4.61

*For all the impurity oxides referred to in this paper the lattice energy refers to the *calculated* value [29].

while the heat of solution based on the neutral trimer (Na^+_{Mg}–V_O–Na^+_{Mg}) is calculated to be 1.58 eV, which is less than 0.2 eV above that for Li_2O. As shown in detail in Table III, then, defect energies associated with impurity substitution in MgO are very similar for Li^+ and Na^+ despite the difference in ion size.

Turning now to interstitial defects, here we do find major differences which can be attributed to the size of the impurity ion in relation to the elastic response of the host lattice. The defect energy of Na^+_I is approximately 5.6 eV greater than that of Li^+_I, so that even though the total binding energy of the neutral {111} trimer, (Na^+_I–V_{Mg}–Na^+_I) is more than 1 eV greater than that of the corresponding Li^+ complex, the calculated heat of solution per Na^+ ion, 3.59 eV, is appreciably higher than that previously found for Li_2O. Furthermore, this is over 2 eV greater than the heat of solution for the anion vacancy trimer, (Na^+_{Mg}–V_O–Na^+_{Mg}) and almost 0.7 eV more than that for free vacancy compensation. Unlike Li^+, therefore, our calculations do not support the existence of Na^+ interstitial defects in MgO.

With regard to surface defects, the present calculations predict that, unlike Li^+, both free Na^+_{Mg} and the neutral vacancy-trimer have lower energies at the surface than in the bulk and that for the latter defect in particular the energy difference is nearly 2.8 eV. For the isolated substitution, Na^+_{Mg}, short-range repulsive interactions clearly make a more decisive contribution to the elastic deformation energy than for Li^+ so that the surface is favoured by over 1 eV. Our calculations suggest, therefore, a marked surface enrichment by Na^+, in the form of both isolated substitutions and neutral vacancy trimers. We conclude, therefore, that in the absence of oxygen exchange, at least, the doping of MgO by Na_2O is much simpler than that by Li_2O. We predict that Na^+ is present solely as a substitution defect compensated by anion vacancies, either free or in association with the impurity depending on the temperature and that at thermal equilibrium there should be an appreciable enrichment of the surface by Na^+.

As is the case with Li^+ the majority of experimental reports refer to oxidized MgO and in particular to the V^0_{Na} centre. We will present calculations for these defects in a separate report [42].

TABLE III Doping of MgO by Na^+. Lattice energy of Na_2O = – 27.10 eV

	(eV)
(a) Bulk defects	
(i) *Na^+ substitution*	
Defect energy of Na^+_{Mg}	18.64
Calculated heat of solution per Na^+ ion	
Free anion vacancy compensation	2.90
Free cation interstitial compensation	5.02
Defect energy of {100} (Na^+_{Mg}–V_O) complex	40.23
Interaction energy of free Na^+_{Mg} and V_O	– 1.32
Defect energy of {100} (Na^+_{Mg}–V_O–Na^+_{Mg}) complex	57.56
Interaction energy of Na^+_{Mg} and (Na^+_{Mg}–V_O)	– 1.31
Total interaction energy of two Na^+_{Mg} and V_O	– 2.63
Calculated heat of solution per Na^+ ion	1.58
(ii) *Na^+ interstitial*	
Defect energy of Na^+_I	2.41
Calculated heat of solution per Na^+ ion	
Free cation vacancy compensation	5.76
Free anion interstitial compensation	12.09
Defect energy of {111} (Na^+_I–V_{Mg}–Na^+_I)	20.82
Total interaction energy of two Na^+_I and V_{Mg}	– 9.41
Calculated heat of solution per Na^+	3.59
(b) {001} surface defects	
Defect energy of Na^+_{Mg}	17.59
Defect of energy of (Na^+_{Mg}–V_O–Na^+_{Mg})	54.79
Total interaction energy of two Na^+_{Mg} and V_O in the {001} surface plane	– 4.44

3.3. Be^{2+}

The first of the isovalent impurities we consider in this paper is Be^{2+}. While the parent oxide, namely BeO, is generally thought to be a somewhat covalent material, we argue that the ionicity of the host lattice should ensure that Be^{2+} in MgO can be treated as a typical ionic impurity as far as the defect structure is concerned. The heat of solution, on the other hand, does depend on the parent oxide and here we have calculated two theoretical values for the lattice energy of BeO. The first, indexed as (a) in Table IV, is based on a straightforward application of the electron-gas model to BeO: that is to say the wave function for Be^{2+} is the free ion value while that for O^{2-} is based on the Madelung potential for an ionic BeO structure [29]. However, the calculated lattice energy, −49.9 eV, is approximately 2 to 3 eV lower than the reported range of −46.5 to −47.5 eV [43], which leads to heats of solution that are unreasonably high. As an alternative procedure we have used the O^{2-} wavefunction for MgO to calculate the cohesive energy of BeO and obtain a value of −47.01 eV which is in much better agreement with experiment. Heats of solution based on this second value for the lattice energy are indexed as (b) in Table IV.

Turning now to the defect structure, the energies associated with Be^{2+} substitution in the bulk have been considered previously [30]: here we extend the range of calculations to include the interstitial impurity and substitution at the {0 0 1} surface. Despite its small size, the interstitial incorporation of Be^{2+} in MgO is predicted to be highly unfavourable compared with substitution. For the latter mode the calculated heat of solution, 2.69 eV, is slightly lower than that for Li^+ and Na^+ (2.78 and 2.90 eV, respectively) in the absence of impurity–defect association which suggests that at high temperatures the solubility of the three ions would be about the same. As mentioned before [30], there is an appreciable interaction (−1.48 eV) between Be_{Mg}^{2+} and cation vacancies, which should lead to a noticeable reduction in the diffusion coefficient and activation energy for migration of Mg^{2+} vacancies. The reason for this large interaction lies in the elastic deformation of the lattice surrounding the separate defects. In the case of Be_{Mg}^{2+} there is a marked contraction of the lattice whereas cation vacancies give rise to a local expansion. In the {1 1 0} dimer configuration the two effects lead to an enhanced relaxation of the surrounding lattice and hence to a considerable binding between the two defects.

Be_{Mg}^{2+} is predicted to be slightly more stable in the bulk than at the {0 0 1} surface and the reason for this is similar to that for the stability of impurity vacancy dimer. At a non-defective surface there is a slight dilation of the lattice by comparison with the bulk, so that the elastic deformation energy required to equilibrate the ions surrounding Be_{Mg}^{2+} is greater at the surface than in the bulk. However, the energy difference between the two, − 0.23 eV, is small and is unlikely to induce a noticeable depletion of the surface impurity concentration.

TABLE IV Doping of MgO by Be^{2+}. Lattice energy of BeO = −49.4 eV (a)*; = −47.01 eV (b)

	(eV)
(a) Bulk defects	
(i) *Be^{2+} substitution*	
Defect energy of Be_{Mg}^{2+}	−3.57
Calculated heat of solution per Be^{2+} ion	5.08 (a)
	2.69 (b)
Defect energy of {1 1 0} (Be_{Mg}^{2+}–V_{Mg})	20.36
Interaction energy of free Be_{Mg}^{2+} and V_{Mg}	−1.48
(ii) *Be^{2+} interstitial*	
Defect energy of Be_i^{2+}	−22.80
Calculated heat of solution per Be^{2+}	11.26 (a)
Free cation vacancy compensation	8.87 (b)
Free anion interstitial compensation	18.86 (a)
	16.47 (b)
(b) {0 0 1} surface defects	
Defect energy of Be_{Mg}^{2+}	−3.80

*Heats of solution marked (a) refer to a lattice energy of −49.90 eV; those marked (b) to one of −47.01 eV. Calculated lattice energies taken from Mackrodt and Stewart [30].

TABLE V Doping of MgO by Ca^{2+}. Lattice energy of CaO = − 36.0 eV

	(eV)
(a) Bulk defects	
Defect energy of Ca^{2+}_{Mg}	5.82
Calculated heat of solution per Ca^{2+} ion	1.07
Defect energy of {1 1 0} Ca^{2+}_{Mg}–V_{Mg}	31.04
Interaction energy of free Ca^{2+}_{Mg} and V_{Mg}	− 0.17
Defect energy of {1 0 0} Ca^{2+}_{Mg}–V_{Mg}	31.61
Interaction energy of free Ca^{2+}_{Mg} and V_{Mg}	0.40
(b) {0 0 1} surface defect	
Defect energy of Ca^{2+}_{Mg}	4.42

3.4. Ca^{2+}

The bulk doping of MgO by Ca^{2+} has been discussed on a previous occasion [30], so that we simply review the situation briefly, adding one or two details not given before. All the relevant defect energies are listed in Table V. Unlike the corresponding dimer involving Be^{2+}_{Mg}, the {1 1 0} Ca^{2+}_{Mg} vacancy associate is only weakly bound (− 0.17 eV) and unlikely to contribute appreciably to the defect properties of MgO in the temperature range at which CaO has a significant solubility. Furthermore, the {1 0 0} dimer is found to be unstable with respect to the isolated point defects. However, our principal finding reported here is that the defect energy of Ca^{2+}_{Mg} is considerably lower at the {0 0 1} surface of MgO than in the volume of the crystal. In addition, the magnitude of this energy difference, 1.40 eV, serves as a good illustration of the importance of lattice relaxation, particularly in surface calculations which are extremely sensitive to small displacements of the outermost ions. The defect energy of Ca^{2+}_{Mg} in the bulk is 5.82 eV so that in the absence of any dilation on the non-defective surface the defect energy would be close to 0.97 eV or less. The added stability of nearly half an electron volt is due entirely to the increased lattice spacing at the surface which reduces the elastic strain energy still further. Our calculations suggest, therefore, that there should be a substantial enrichment of the surface of MgO by Ca^{2+} at thermal equilibrium. This is precisely the situation reported recently by Wynblatt and McCune [23] who find strong segregation at the {0 0 1} surface of MgO crystals containing 220 ppm calcium. From these data they deduce a heat of segregation of -0.78 ± 0.2 eV. In a separate report [44] we will extend the present calculations to include impurity segregation at the {0 0 1} and {1 1 0} surfaces, thereby enabling direct comparison with the experimental data.

3.5. Fe^{2+}

The doping of MgO by transition metal ions, particularly with regard to the stability and electronic properties of the various charged states that can occur, has been the subject of numerous investigations, most recently by Sangster and Stoneham [45, 46]. Lately, Gourdin and Kingery [12] have also reported energies for Fe^{2+} and Fe^{3+} defects in MgO. A major problem that arises in describing the defect structure of these states concerns the interplay between lattice relaxation and electronic "crystal-field" effects and this will be examined in full in a separate report [42]. For the present we concentrate on those aspects of the doping of Fe^{2+} that rely almost exclusively on lattice energies.

As shown in Table VI the defect energy for Fe^{2+} substitution, 4.33 eV, is appreciably higher than that reported by Gourdin and Kingery [12] and leads to a heat of solution of 0.79 eV. This is probably too low a value by virtue of our theoreti-

TABLE VI Doping of MgO by Fe^{2+}. Lattice energy of FeO = − 37.21 eV

	(eV)
(a) Bulk defects	
Defect energy of Fe^{2+}_{Mg}	4.33 (1.39)*
Calculated heat of solution per Fe^{2+} ion	0.79
Defect energy of {1 1 0} (Fe^{2+}_{Mg}–V_{Mg})	29.84
Interaction energy of free Fe^{2+}_{Mg} and V_{Mg}	0.10
(b) {0 0 1} surface defect	
Defect energy of Fe^{2+}_{Mg}	3.34

*Figures in brackets are the corresponding energies reported by Gourdin and Kingery [12].

cal lattice energy for FeO of −37.2 eV [42] which is somewhat higher than the range quoted by Waddington [47]. However, since all our calculations are based on a consistent set of potentials for MgO, FeO and Fe^{2+}:MgO it is unlikely that our calculated heat of solution is in error by as much as the lattice energy for FeO. We find a small repulsive interaction between Fe^{2+}_{Mg} and a cation vacancy in the {110} configuration, while our results for Ca^{2+} suggest that this is likely to be even greater for the {100} dimer. We predict, therefore, that there is unlikely to be any influence on the activation energy for cation vacancy migration. The calculated defect energy for Fe^{2+} substitution at the surface is 3.34 eV which is approximately 1 eV less than in the bulk. However, here, unlike the case for closed-shell impurities, we need to consider, in addition to the lattice energy, the crystal-field stabilization energy (CFSE), for this could have an important bearing on the overall difference between the bulk and surface-defect energies. A simple analysis leads to the following values for Fe^{2+} (d^6) in MgO [48].

Spin state/location	CFSE
High-spin bulk	$4D_q$
High-spin {001} surface	$4.57D_q$
Low-spin bulk	$24D_q - 5B - 8C$
Low-spin {001} surface	$20D_q - 5B - 8C$

in which D_q, B and C have their usual meaning [48]. For values of D_q of about 0.15 eV [49] the energy difference for the high-spin state is less than 0.1 eV, whereas in the low-spin state the bulk is favoured by about 0.6 eV. Since Fe^{2+} (d^6) is thought to be low spin in FeO [49] we assume the same to be the case in MgO, so that the overall energy difference between the bulk and surface is now approximately 0.4 eV. We predict, therefore, that at thermal equilibrium, the concentration of Fe^{2+} in MgO will be more or less uniform throughout the crystal, but possibly with a slight preference for the bulk.

Black and Kingery [22] have recently reported observations of segregation from iron-containing samples of MgO. In a reducing atmosphere in which the iron is present at Fe^{2+} they found no concentration changes at the surface: thus we find good accord with experiment.

3.6. Al^{3+}

We now consider the first of the trivalent impurities, namely, Al^{3+}, for which there have been two sets of calculations reported recently for bulk defects [12, 30]. The first, and more extensive of the two, by Gourdin and Kingery [12], uses a combination of empirical and non-empirical potentials for MgO [50] and α-Al_2O_3 [51]; the second [30] is based on potentials that are identical to those used here. For completeness we present the full range of calculations for the bulk in addition to those for the surface and compare the results for the two sets of potentials.

In the absence of defect association, Al^{3+} as an impurity substitution can be compensated by either cation vacancies or anion interstitials. However, as Table VII shows the former is by far the more favourable of the two modes, with a calculated heat of solution of 2.24 eV. The value obtained by Gourdin and Kingery [12], 4.1 ± 1.5 eV, is somewhat higher, due principally to a defect energy for Al^{3+}_{Mg} that is over 5 eV greater than that found here. There is an appreciable binding of Al^{3+}_{Mg} to cation vacancies to form both dimers and neutral trimers, but in both cases the {100} defect is the more stable of the two, as found previously [12]. Once again the explanation is similar to that given for the stability of the Be^{2+}_{Mg} vacancy dimer. At equilibrium the six nearest-neighbour anions surrounding an isolated Al^{3+}_{Mg} are displaced towards the defect, whereas they are displaced away from a cation vacancy. In the {100} dimer, therefore, these displacements are exactly in phase, as illustrated in Fig. 5, thereby allowing the central anion the maximum degree of relaxation.In the {100} dimer, on the other hand, the two central anions are acted on by forces that are perpendicular to each other

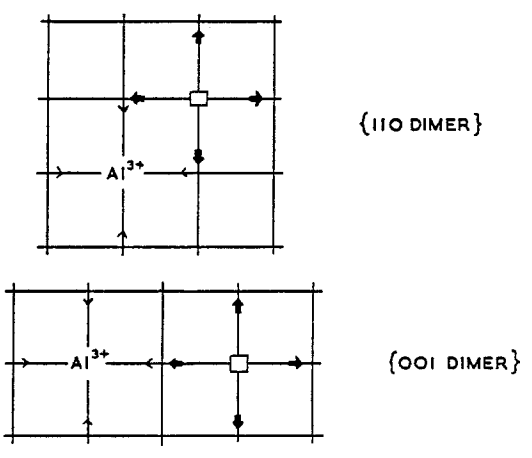

Figure 5 Lattice relaxation at Al^{3+}–V_{Mg} dimers.

TABLE VII Doping of MgO by Al^{3+}. Lattice energy of α-Al_2O_3 = −161.9 eV

	(eV)
(a) Bulk defects	
(i) *Al^{3+} substitution*	
Defect energy of Al^{3+}_{Mg}	−30.29 (−24.98)*
Calculated heat of solution per Al^{3+} ion	
Free cation vacancy compensation	2.24 (4.1 ± 1.5)
Free anion interstitial compensation	6.04
Defect energy of {100} (Al^{3+}_{Mg}–V_{Mg}) complex	−5.76
Interaction energy of Al^{3+}_{Mg} and V_{Mg}	−0.88 (−0.86)
Defect energy of {110} (Al^{3+}_{Mg}–V_{Mg}) complex	−5.41
Interaction energy of free Al^{3+}_{Mg} and V_{Mg}	−0.54 (−0.68)
Defect energy of {100} (Al^{3+}_{Mg}–V_{Mg}–Al^{3+}_{Mg})	36.95
Interaction energy of Al^{3+}_{Mg} and (Al^{3+}_{Mg}–V_{Mg})	−0.90
Interaction energy of two free Al^{3+}_{Mg} and V_{Mg}	−1.79 (−1.68)
Calculated heat of solution per Al^{3+} ion	1.35
Defect energy of {110} (Al^{3+}_{Mg}–V_{Mg}–Al^{3+}_{Mg})	−36.12
Interaction energy of Al^{3+}_{Mg} and (Al^{3+}_{Mg}–V_{Mg})	−0.42
Interaction energy of two free Al^{3+}_{Mg} and V_{Mg}	−0.95 (−1.32)
Calculated heat of solution per Al^{3+}_{Mg} ion	1.77
Defect energy of {111} (Al^{3+}_{Mg}–O_I^{2-}) complex	−38.49
Interaction energy of free Al^{3+}_{Mg} and O_I^{2-}	−0.46
(ii) *Al^{3+} interstitial*	
Defect energy of Al^{3+}_I ion	−43.00 (−33.84)
Calculated heat of solution per Al^{3+} ion	
Free cation vacancy compensation	14.94
Free anion interstitial compensation	26.34
(b) {001} surface defects	
Defect energy of Al^{3+}_{Mg}	−29.77
Defect energy of {110} (Al^{3+}_{Mg}–V_{Mg})	−5.08
Interaction energy with respect to the Al^{3+}_{Mg} and V_{Mg} in the surface	−1.22
Defect energy of {110} (Al^{3+}_{Mg}–V_{Mg}–Al^{3+}_{Mg})	−35.29
Interaction energy with respect to {110} (Al^{3+}_{Mg}–V_{Mg}) and V_{Mg} in the surface	−0.44
Interaction energy with respect to two free Al^{3+}_{Mg} and V_{Mg} in the {001} surface	−1.66

*The figures in brackets are the corresponding energies reported by Gourdin and Kingery [12].

thereby limiting the extent of lattice stabilization. This is essentially the argument given by Gourdin and Kingery [12] in their discussion of Al^{3+} vacancy complexes; however, as shown later, this argument leads to the reverse order for the stability of impurity–vacancy dimers involving Sc^{3+} and Fe^{3+}. The {100} associate is bound by approximately 0.2 eV more than the {110} complex, while the difference for the corresponding trimer is found to be almost 0.9 eV. For the {100} defects the present calculations predict interaction energies that are slightly greater than those given by Gourdin and Kingery [12], whereas it is the reverse for the {110} associates. However, in each case the agreement between the two sets of calculations is remarkably close, despite the fact that the energies for the *individual* defects differ quite substantially.

We have also considered the association of Al^{3+}_{Mg} and an O^{2-} interstitial as a possible means of stabilizing anion Frenkel defects in MgO, but find that the interaction energy is less than 0.5 eV. With regard to Al^{3+} interstitials, our calculations suggest a similar situation to that predicted for Be^{2+}. That is to say, despite the small size of the Al^{3+} ion, impurity interstitials compensated by either cation vacancies or anion interstitials remain highly unfavourable from an energetic point of view, with heat of solution of 14.94 and 26.34 eV per Al^{3+} ion in the absence of defect association. Once again this view accords with that previously found [12]. The defect energies of Al^{3+}_{Mg} and the {100} dimer and trimer are all predicted to be lower in the bulk than at the {001} surface, with differences ranging from approximately half an electron volt for the isolated

substitution to 1.66 eV in the case of the neutral trimer. For the two charged defects the Madelung potential in combination with the long-range polarization and local contraction of the lattice favour the bulk and these evidently compensate for the reduction in the repulsive potential at the surface. The relative stability of the neutral trimer, on the other hand, is determined solely by the local contraction of the lattice which is clearly not favoured at the relaxed surface. We conclude from these calculations, then, that for MgO doped with Al^{3+}, there will be a depletion of the impurity concentration at the surface relative to the bulk.

We cannot compare our present calculations directly with experiment, for Al^{3+} segregation at the surface is accompanied by spinel formation [25, 26] which we cannot treat as yet. However, we note that for the bulk our calculated value for the energy of formation of spinel from MgO and Al_2O_3 is -0.95 eV.

3.7. Sc^{3+}

The second of the trivalent impurities we consider in this paper is Sc^{3+} for which the appropriate bulk and surface defect energies are listed in Table VIII. Unlike the situation for the other impurities our computational procedures have not been able to cope with the very large unit cell of the parent oxide, Sc_2O_3, so that we are unable to estimate heats of solution. Our analysis, therefore, is confined solely to defect energies.

By comparison with Al^{3+} these are approximately 8 eV higher per impurity ion due to the increased short range repulsion of Sc^{3+}. The binding energies of the various dimers and trimers, on the other hand, we find to be of the same order of magnitude. Now apart from the differences in the absolute energies just referred to, the relative energies of the {1 0 0} and {1 1 0} associates are also quite different from the corresponding Al^{3+} complexes, for here the {1 1 0} defects are predicted to be the more stable of the two. Much the same sort of reasoning applies here as for Al^{3+}. However,

TABLE VIII Doping of MgO by Sc^{3+}

	(eV)
(a) Bulk defects	
Defect energy of $Sc^{\cdot}_{Mg}$	−22.29
Defect energy of {1 0 0} ($Sc^{\cdot}_{Mg}$–V_{Mg})	2.51
Interaction energy of $Sc^{\cdot}_{Mg}$ and V_{Mg}	−0.61
Defect energy of {1 1 0} ($Sc^{\cdot}_{Mg}$–V_{Mg})	2.33
Interaction energy of $Sc^{\cdot}_{Mg}$ and V_{Mg}	−0.79*
Defect energy of {1 0 0} ($Sc^{\cdot}_{Mg}$–V_{Mg}–$Sc^{\cdot}_{Mg}$)	−20.35
Interaction energy of $Sc^{\cdot}_{Mg}$ and ($Sc^{\cdot}_{Mg}$–V_{Mg})	−0.57
Interaction energy of two $Sc^{\cdot}_{Mg}$ and V_{Mg}	−1.18
Defect energy of {1 1 0} ($Sc^{\cdot}_{Mg}$–V_{Mg}–$Sc^{\cdot}_{Mg}$)	−20.71
Interaction energy of $Sc^{\cdot}_{Mg}$ and ($Sc^{\cdot}_{Mg}$–V_{Mg})	−0.75
Interaction energy of two free $Sc^{\cdot}_{Mg}$ and V_{Mg}	−1.54
Defect energies of {1 1 1} ($Sc^{\cdot}_{Mg}$–O^{2}_{I})	−31.57
Interaction energy of $Sc^{\cdot}_{Mg}$ and O^{2-}_{I}	−1.54
(b) {0 0 1} surface defects	
Defect energy of $Sc^{\cdot}_{Mg}$	−21.78
Defect energy of {1 1 0} ($Sc^{\cdot}_{Mg}$–V_{Mg}) in the surface	1.66
Interaction energy of $Sc^{\cdot}_{Mg}$ and V_{Mg} in the surface	−2.47
Interaction energy of {1 1 0} ($Sc^{\cdot}_{Mg}$–V_{Mg}) in the surface with respect to $Sc^{\cdot}_{Mg}$ and V_{Mg} in the bulk	−1.46
Defect energy of {1 1 0} ($Sc^{\cdot}_{Mg}$–V_{Mg}) perpendicular to {0 0 1} surface–V_{Mg} in surface plane	1.76
Defect energy of {1 1 0} ($Sc^{\cdot}_{Mg}$–V_{Mg}–$Sc^{\cdot}_{Mg}$)	−21.59
Interaction energy of two $Sc^{\cdot}_{Mg}$ and V_{Mg} in the surface	−3.94
Interaction energy of {1 1 0} ($Sc^{\cdot}_{Mg}$–V_{Mg}) and $Sc^{\cdot}_{Mg}$ in the surface plane	−1.47
Interaction energy of {1 1 0} ($Sc^{\cdot}_{Mg}$–V_{Mg}–$Sc^{\cdot}_{Mg}$) in the surface with respect to {1 1 0} ($Sc^{\cdot}_{Mg}$–V_{Mg}) in the surface and $Sc^{\cdot}_{Mg}$ in the bulk	−0.96
Interaction energy of {1 1 0} ($Sc^{\cdot}_{Mg}$–V_{Mg}–$Sc^{\cdot}_{Mg}$) in the surface with respect to 2 $Sc^{\cdot}_{Mg}$ and V_{Mg} in bulk	−2.42

*Experimental value 0.73 eV [4].

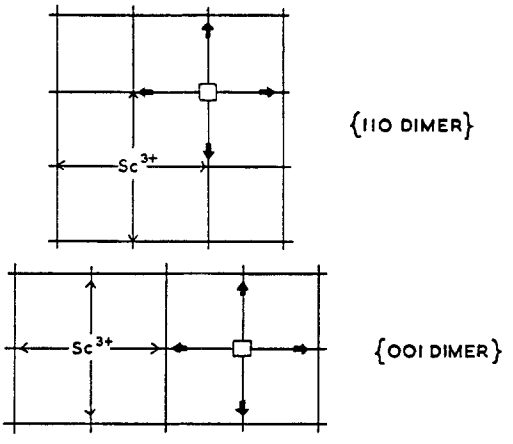

Figure 6 Lattice relaxation at Sc^{3+}–V_{Mg} dimers.

the difference is that in this case the nearest neighbour anions surrounding both the cation vacancy and Sc^{3+}_{Mg} are displaced outwards, so that in the {1 0 0} dimer, the central ion is under the influence of opposing repulsive forces thereby limiting the extent to which the strain energy of the complex can be lowered by lattice relaxation. As shown in Fig. 6, this is not the case for the {1 1 0} dimer; however, the energy differences between the configurations are quite small being approximately 0.2 eV for the dimer and 0.4 eV for the corresponding trimers. With regard to experiment, we note with interest that our calculated binding energy of the {1 1 0} dimers, 0.79 eV, is in very good agreement with the value of 0.73 eV recently reported by Sempolinski and Kingery [4].

A further example of the differences between Sc^{3+} and Al^{3+} substitution is the interaction energy with an O^{2-} interstitial. For Sc^{3+}_{Mg} it is calculated to be −1.54 eV which is appreciably greater than that found for Al^{3+}_{Mg} (− 0.46 eV) and, once again, lattice relaxation effects are responsible for this difference. There is a local outward displacement of the ions surrounding an O^{2-} interstitital which is enhanced by the presence of a neighbouring Sc^{3+} ion, but diminished by Al^{3+}. Unlike the vacancy dimers and trimers, however, all the surrounding ions are subject to these combined forces so that the overall difference in energy between the two cases is quite appreciable.

Turning now to surface defects and in particular to the differences between the bulk and the surface, we find a more complex situation here than for any previous impurity as shown in Table VIII. The isolated substitution, Sc^{3+}_{Mg}, is found to be more stable in the bulk by virtue of the Madelung potential which is always greater in the bulk than at the surface. The {1 1 0} vacancy dimer and trimer, on the other hand, are calculated to have lower energies at the surface, in contrast to the corresponding Al^{3+} associates. In the case of the dimer this is true for configurations in which the dimer is both in the surface plane and perpendicular to it. If we now consider the binding energies of these associates, that is to say the energy differences between the associates and the separated vacancy and Sc^{3+} substitutions, the values we get clearly depend on the location of the separated defects. For example, the binding energy of the {1 1 0} dimer in the surface plane with respect to the vacancy and Sc^{3+}_{Mg} also in the surface plane is − 2.47 eV; however, this is reduced by over 1 eV for separated defects in the bulk. For the {1 1 0} trimer in the surface plane the corresponding difference is even greater at over 1.5 eV. Thus we have two sets of dissociation energies for the dimer and trimer. The first, which might be referred to as the "non-equilibrium" values, corresponds to the separated defects in the surface, whereas the second, which we designate as the "equilibrium" values, refer to the isolated defects in the bulk. Then for the two processes, we have the situation as shown in Table IX.

Now the important point here is that the difference in the dissociation energies for the two processes is large, irrespective as to whether we choose the "equilibrium" or "non-equilibrium"

TABLE IX

	ΔE (eV)	
	"Non-equilibrium"	"Equilibrium"
$(Sc^{3+}_{Mg}–V_{Mg}–Sc^{3+}_{Mg}) \rightarrow (Sc^{3+}_{Mg}–V_{Mg}) + Sc^{3+}_{Mg}$	1.47	0.96
and		
$(Sc^{3+}_{Mg}–V_{Mg}) \rightarrow Sc^{3+}_{Mg} + V_{Mg}$	2.47	1.46
Energy difference for the two processes	1.0	0.5

values; and certainly much larger than the corresponding difference in the bulk which is only 0.04 eV. We predict, therefore, that at the surface, the first of the two processes, namely the dissociation of the trimer, dominates and that this will lead to the formation of a negative space charge region at the surface, since $(Sc_{Mg}^{3+}-V_{Mg})$ is more stable at the surface, whereas Sc_{Mg}^{3+} has a lower energy in the bulk.

Black and Kingery [22] have recently found excess Sc^{3+} at the {0 0 1} surface of MgO so that here we find good agreement with experiment for both the bulk and surface defects.

3.8. Fe^{3+}

The final trivalent impurity we consider in this report is Fe^{3+}, for which the calculated defect energies are given in Table X. We assume Fe_{Mg}^{3+} to be in a high-spin d^5 state so that all our results here, like those for Fe^{2+}, are independent of crystal-field effects. On the whole the situation is very similar to that for Sc^{3+}, particularly so in the bulk, with differences of little more than 0.2 eV for any of the individual defects. The present results, however, differ quite markedly from those reported by Gourdin and Kingery [12] in a number of respects. The energy of Fe^{3+} substitution is over 7 eV greater than that previously found and this is largely responsible for the difference in the two heats of solution for free cation vacancy compensation. Here we find a value of 3.54 eV as opposed to one of -2.9 ± 3 eV given earlier [12]. There is good agreement for the binding energies of the {1 1 0} dimer and trimer, but the two sets of calculations are at variance both with regard to the relative stability of the {1 1 0} and {1 0 0} associates and the binding energies of the latter. Here we predict the

TABLE X Doping of MgO by Fe^{3+}. Lattice energy of α-$Fe_2O_3 = -148.7$ eV

	(eV)
(a) Bulk defects	
Defect energy of Fe_{Mg}^{3+}	−22.39 (−29.67)*
Calculated heat of solution per Fe^{3+} ion	
Free cation vacancy compensation	3.54 (−2.9 ± 3)
Free anion interstitial compensation	7.34
Defect energy of {1 0 0} $(Fe_{Mg}^{3+}-V_{Mg})$	2.42
Interaction energy of Fe_{Mg}^{3+} and V_{Mg}	−0.60 (−1.13)
Defect energy of {1 1 0} $(Fe_{Mg}^{3+}-V_{Mg})$	2.23
Interaction energy of Fe_{Mg}^{3+} and V_{Mg}	−0.79 (−0.88)
Defect energy of {1 0 0} $(Fe_{Mg}^{3+}-V_{Mg}-Fe_{Mg}^{3+})$	−20.53
Interaction energy of Fe_{Mg}^{3+} and $(Fe_{Mg}^{3+}-V_{Mg})$	−0.56
Interaction energy of two Fe_{Mg}^{3+} and V_{Mg}	−1.16 (−2.20)
Calculated heat of solution per Fe^{3+} ion	2.96
Defect energy of {1 1 0} $(Fe_{Mg}^{3+}-V_{Mg}-Fe_{Mg}^{3+})$	−20.91
Interaction energy of Fe_{Mg}^{3+} and $(Fe_{Mg}^{3+}-V_{Mg})$	−0.75
Interaction energy of two Fe_{Mg}^{3+} and V_{Mg}	−1.54 (−1.42)
Calculated heat of formation per Fe^{3+} ion	2.77
Defect energy of {1 1 1} $(Fe_{Mg}^{3+}-O_I^{2-})$	−31.68
Interaction energy of Fe_{Mg}^{3+} and O_I^{2-}	−1.54
(b) {0 0 1} surface defects	
Defect energy of Fe_{Mg}^{3+}	−22.25
Defect energy of {1 1 0} $(Fe_{Mg}^{3+}-V_{Mg})$ in the surface	1.56
Interaction energy of Fe_{Mg}^{3+} and V_{Mg} in the surface	−2.10
Interaction energy of {1 1 0} $(Fe_{Mg}^{3+}-V_{Mg})$ in the surface with respect to Fe_{Mg}^{3+} and V_{Mg} in the bulk	−1.46
Defect energy of {1 1 0} $(Fe_{Mg}^{3+}-V_{Mg}-Fe_{Mg}^{3+})$	−3.19
Interaction energy of {1 1 0} $(Fe_{Mg}^{3+}-V_{Mg})$ in the surface	−1.09
Interaction energy of {1 1 0} $(Fe_{Mg}^{3+}-V_{Mg}-Fe_{Mg}^{3+})$ in the surface with respect to {1 1 0} $(Fe_{Mg}^{3+}-V_{Mg})$ in the surface and Fe_{Mg}^{3+} in the bulk	−0.95
Interaction energy of {1 1 0} $(Fe_{Mg}^{3+}-V_{Mg}-Fe_{Mg}^{3+})$ in the surface with respect to 2 Fe_{Mg}^{3+} and V_{Mg} in the bulk	−2.41

*Figures in brackets are the corresponding energies reported by Gourdin and Kingery [12].

{1 1 0} defects to be the more stable of the two by about 0.2 eV per Fe^{3+}_{Mg}–V_{Mg} interaction, for reasons similar to those given for Sc^{3+}; whereas the previous calculations suggest the reverse order of stability with an energy difference of about 0.4 eV. Allowing for impurity–vacancy interaction, then, the present calculations predict a heat of solution in the range 2.77 to 3.54 eV, depending on the degree of association, in contrast to those of [12] which lead to one of between -2.9 ± 3 and -4.0 ± 3.0 eV. We have also considered the interaction between Fe^{3+}_{Mg} and an O^{2-} interstitial and although the two are bound by over 1.5 eV this is insufficient to render this mode of compensation favourable, for the heat of solution is still well over 5 eV.

While it is not our intention here to consider the stability of the various charged states in detail, from the defect energies of Fe^{2+}_{Mg} and Fe^{3+}_{Mg} we can calculate the enthalpy, ΔE, for the *thermal process,*

$$Fe^{2+}_{Mg} \rightarrow Fe^{3+}_{Mg} + e_c$$

in which the excitation is to the conduction band, and from this estimate the position of the Fe^{2+}/Fe^{3+} level in the band-gap. Using values of -0.7 eV for the conduction-band edge given previously [30] and the free-ion ionization potential of 30.65 eV [52], we find ΔE to be 3.23 eV. This locates the impurity level at roughly the middle of the thermal band-gap which has previously been estimated to be 6.0 eV [30] based on calculations similar to those reported here.

Sempolinski *et al.* [1] have recently reported experimental values of 3.32 ± 0.52 and 6.8 ± 0.5 eV for the excitation energy and thermal band gap, respectively, which further confirms the general validity of the present calculations.

The surface defect structure associated with Fe^{3+} is yet another example of the diversity of effects that result from cation doping. The relative bulk/surface stability of the vacancy associates is similar to that for Sc^{3+} in that both the dimer and trimer are lower in energy at the surface. Once again we find quite appreciable binding energies for these associates. For example, the {1 1 0} trimer is bound by 0.95 eV with respect to the surface dimer which in turn is bound by 1.46 eV with respect to the isolated defects in the bulk. However, the difference in energy for the isolated defect Fe^{3+}_{Mg}, between the surface and the bulk (0.14 eV) is very much smaller than that for Sc^{3+} (0.51 eV) so that here we predict surface enrichment by Fe^{3+} at thermal equilibrium, but without an enhancement of a negative space-charge layer found for Sc^{3+}. Thus we predict appreciable differences between the solubility of FeO and α-Fe_2O_3 in MgO and also in the surface to bulk enrichment for Fe^{2+}_{Mg} and Fe^{3+}_{Mg}. Once again our predicted enrichment of the {0 0 1} surface is in agreement with the experimental data of Black and Kingery [22].

3.9. Ti^{4+}

The first of the quadrivalent impurities we consider in this paper is Ti^{4+} for which similar calculations involving the doping of α-Al_2O_3 have recently been reported [53, 54]. The present results are collected in Table XI. For Ti^{4+} substitution, vacancy compensation is predicted to be the more favoured of the two possible modes by far, although the heat of solution is high at over 7 eV. The inclusion of vacancy–impurity dimers reduces this to 5.70 eV per Ti^{4+} ion, but nonetheless our calculations suggest that at all but the highest temperatures the solubility of TiO_2 in MgO will be small. We note that the corresponding solubility in α-Al_2O_3 is predicted to be much greater, with heats of solution varying from 1.79 to 3.53 eV depending on the degree of aggregation [54]. Ti^{4+} interstitials, although highly stable as isolated defects, require over 10 eV for solution from TiO_2, even allowing for impurity clustering, so that here too we expect the concentration to be extremely low. In line with other highly charged defects, Ti^{4+}_{Mg} is more stable in the bulk than at the surface, in this case by nearly 2 eV, but, as before, the dimer is predicted to have a lower energy at the surface. However, unlike (Sc^{3+}_{Mg}–V_{Mg}), this applies only to the Ti^{4+} dimer in a configuration in which it is perpendicular to the surface plane. The calculated energy difference between this state and the bulk seems to be rather large and this we suspect might be due to the low symmetry of the defect at the surface and hence to the reduced number of ions in the inner region. We find the surface dimer to be tightly bound by about 5 eV with respect to the equilibrium location of Ti^{4+}_{Mg} and the cation vacancy, so that our calculations predict a marked surface enrichment by this impurity in the form of neutral defects without any tendency to form a space-charge layer.

3.10. Si^{4+}

The final impurity we consider in the paper is

TABLE XI Doping of MgO by Ti^{4+}. Lattice energy of $TiO_2 = -122.40$ eV

	(eV)
(a) Bulk defects	
(i) *Ti^{4+} substitution*	
Defect energy of Ti^{4+}_{Mg}	−59.25
Calculated heat of solution per Ti^{4+}_{Mg}	
Free cation vacancy compensation	7.06
Free anion interstitial compensation	14.66
Defect energy of $\{100\}$ $(Ti^{4+}_{Mg}–V_{Mg})$	−35.20
Interaction energy of Ti^{4+}_{Mg} and V_{Mg}	−1.36
Calculated heat of solution per Ti^{4+} ion	5.70
(ii) *Ti^{4+} interstitial*	
Defect energy of Ti^{4+}_{I}	−65.36
Calculated heat of solution per Ti^{4+} ion	
Free cation vacancy compensation	26.36
Free anion interstitial compensation	41.57
Defect energy of $(V_{Mg}–Ti^{4+}_{I}–V_{Mg})$	−30.42
Interaction energy of 2 V_{Mg} and Ti^{4+}_{I}	−15.88
Calculated heat of solution per Ti^{4+} ion	10.48
(b) $\{001\}$ surface defects	
Defect energy of Ti^{4+}_{Mg}	−57.28
Defect energy of $\{110\}$ $(Ti^{4+}_{Mg}–V_{Mg})$ in surface (a)	−35.00
Defect energy of $\{110\}$ $(Ti^{4+}_{Mg}–V_{Mg})$ perpendicular to surface plane with Ti^{4+}_{Mg} in the surface (b)	−38.78
Interaction energy of Ti^{4+}_{Mg} and V_{Mg} in the surface (a)	−3.43
Interaction energy of Ti^{4+}_{Mg} and V_{Mg} in the surface (b)	−7.21
Interaction energy of $\{110\}$ $(Ti^{4+}_{Mg}–V_{Mg})$ in the surface (a) with respect to Ti^{4+}_{Mg} and V_{Mg} in the bulk	−1.16
Interaction energy of $\{110\}$ $(Ti^{4+}_{Mg}–V_{Mg})$ in the surface (b) with respect to Ti^{4+}_{Mg} and V_{Mg} in the bulk	−4.94

Si^{4+}, for which the appropriate defect energies are given in Table XII. As was the case for Be^{2+}, it is important to emphasize that while it is clear that SiO_2 is a completely covalent material, Si^{4+} as an impurity in MgO might, to a first approximation, be treated as an ionic impurity; and that provided the calculations are interpreted with caution they might be of interest both in relation to the other impurities discussed here and also to experiment. Broadly speaking the results parallel those for Ti^{4+}, with cation vacancy compensation being the preferred mode for Si^{4+} substitution. The $\{100\}$ dimer is predicted to be more stable than the $\{110\}$ for reasons similar to those given for Al^{3+}, with a binding energy of nearly 1.5 eV. Si^{4+} as an interstitial defect is highly stable and very strongly bound to cation vacancies. However, as in the case of Ti^{4+}, the total energy is still greater than that for the corresponding substitutional defect by about 5 eV. Isolated Si^{4+}_{Mg} is calculated to be more stable in bulk than at the surface, but as before the dimer, which is tightly bound by about 3.5 eV, has a lower energy at the $\{001\}$ surface. Bearing in mind our previous remarks, then, our calculations suggest a surface enrichment of MgO by Si^{4+} as the neutral $\{110\}$ vacancy dimer.

TABLE XII Doping of MgO by Si^{4+}

	(eV)
(a) Bulk defects	
(i) *Si^{4+} substitution*	
Defect energy of Si^{4+}_{Mg}	−68.91
Defect energy of $\{110\}$ $(Si^{4+}_{Mg}–V_{Mg})$	−44.61
Interaction energy of Si^{4+}_{Mg} and V_{Mg}	−1.11
Defect energy of $\{100\}$ $(Si^{4+}_{Mg}–V_{Mg})$	−44.98
Interaction energy of Si^{4+}_{Mg} and V_{Mg}	−1.48
Defect energy of $\{111\}$ $(Si^{4+}_{Mg}–O^{2-}_{I})$	−78.18
Interaction of Si^{4+}_{Mg} and O^{2-}_{I}	−1.53
(ii) *Si^{4+} interstitial*	
Defect energy of Si^{4+}_{I}	−77.38
Defect energy of $(V_{Mg}–Si^{4+}_{I}–V_{Mg})$	−39.06
Interaction energy of Si^{4+}_{I} and two V_{Mg}	−12.50
(b) $\{001\}$ *surface defects*	
Defect energy of Si^{4+}_{Mg}	−67.43
Defect energy of $\{110\}$ $(Si^{4+}–V_{Mg})$	−45.05

3.11. Impurity–impurity interactions in MgO

Here we consider rather briefly the interaction

between Li^+ and Na^+, on the one hand, and the highly charged cations Al^{3+}, Sc^{3+}, Fe^{3+} and Si^{4+}. The calculated defect energies are listed in Table XIII. As indicated the binding energies are small and certainly less than the corresponding vacancy interactions. For crystals doped with impurities of this type, therefore, our calculations suggest little interaction between them, particularly so at high temperature.

4. Summary of defect calculations

To summarize our defect calculations, then, we find a diversity of effects both in the bulk and surface of MgO doped by the various cation impurities considered. We find differences that are due solely to size effects, such as those between Li^+ and Na^+ and Al^{3+} and Sc^{3+} and others that result from the charge state of the impurity, such as Fe^{2+} and Fe^{3+}. From our calculated heats of solution we predict the relative order of solubility in MgO at high temperatures to be

$$FeO > CaO > \alpha\text{-}Al_2O_3 > BeO > Li_2O > Na_2O > \alpha\text{-}Fe_2O_3 > TiO_2.$$

However, our calculations suggest that this will be markedly different at temperatures which permit defect association. We predict a range of binding energies for the various dimers and trimers that can be formed from 0.17 eV for the {1 1 0} vacancy dimer, $(Ca^{2+}_{Mg}-V_{Mg})$, to 15.88 eV for the interaction energy of Ti_I^{4+} and two cation vacancies. In the case of Li^+ in the absence of oxygen exchange, we predict an interstitial impurity of the type proposed for Li^+:MgF_2 and suggest that similar dielectric relaxation effects should result. Our calculations also suggest that at thermal equilibrium there should be a surface enrichment of MgO by Na^+, Ca^{2+}, Sc^{3+}, Ti^{4+} and Si^{4+} and that in the case of Sc^{3+} this should be accompanied by the formation of a space-charge region. We find little interaction between monovalent and trivalent impurities, which suggests that the defect structure associated with each type can be treated separately. Finally, we note with interest the good agreement between our calculated defect energies and the available experimental data. This lends support to the overall validity of a computational approach to defect structures in ionic materials.

TABLE XIII Impurity–impurity interactions in MgO

	(eV)
Defect energy of $(Li^{+}_{Mg}-Al^{3+}_{Mg})$	−14.29
Interaction energy of Li^{+}_{Mg} and Al^{3+}_{Mg}	−0.27
Defect energy of $(Li^{+}_{Mg}-Sc^{3+}_{Mg})$	−6.52
Interaction energy of Li^{+}_{Mg} and Sc^{3+}_{Mg}	−0.41
Defect energy of $(Li^{+}_{Mg}-Fe^{3+}_{Mg})$	−6.43
Interaction energy of Li^{+}_{Mg} and Fe^{3+}_{Mg}	−0.41
Defect energy of $(Na^{+}_{Mg}-Al^{3+}_{Mg})$	−11.90
Interaction energy of Na^{+}_{Mg} and Al^{3+}_{Mg}	−0.25
Defect energy of $(Na^{+}_{Mg}-Sc^{3+}_{Mg})$	−4.00
Interaction energy of Na^{+}_{Mg} and Sc^{3+}_{Mg}	−0.35
Defect energy of $(Na^{+}_{Mg}-Fe^{3+}_{Mg})$	−4.10
Interaction energy of Na^{+}_{Mg} and Fe^{3+}_{Mg}	−0.35
Defect energy of $Na^{+}_{Mg}-Si^{4+}_{Mg}-Na^{+}_{Mg}$	−32.44
Interaction energy of two Na^{+}_{Mg} and Si^{4+}_{Mg}	−0.81

References

1. D. R. SEMPOLINSKI, W. D. KINGERY and H. L. TULLER, *J. Amer. Ceram. Soc.* **63** (1980) 669.
2. R. A. WEEKS and E. SONDER, *Rev. Int. Hautes Temp. Refract. Fr.* **17** (1980) 154.
3. A. M. STONEHAM, M. J. L. SANGSTER and P. W. TASKER, *Phil. Mag.* **B44** (1981) 603.
4. D. R. SEMPOLINSKI and W. D. KINGERY, *J. Amer. Ceram. Soc.* **63** (1980) 664.
5. M. DUCLOT and C. DEPORTES, *J. Solid State Chem.* **31** (1980) 377.
6. O. GONCHAROVA and T. M. YURIEVA, *React. Kinet. Catal. Lett.* **15** (1980) 73.
7. C. ANGELETTI, A. CIMENO, V. INDOVINA, F. PEPE and M. SCHIAVELLO, *J. Chem. Soc. Faraday Trans. I* **77** (1981) 641.
8. A. B. LIDIARD and M. J. NORGETT, in "Computational Solid State Physics", edited by F. H. Herman, N. W. Dalton and T. R. Koehler (Plenum, New York, 1971).
9. M. J. NORGETT, A.E.R.E. Report: AERE-R7015 (1972).
10. *Idem*, A.E.R.E. Report: AERE-R7605 (1974).
11. C. R. A. CATLOW and W. C. MACKRODT, in "Computer Simulation of Solids", edited by C. R. A. Catlow and W. C. Mackrodt (Springer-Verlag, Berlin, 1982).
12. W. H. GOURDIN and W. D. KINGERY, *J. Mater. Sci.* **14** (1979) 2053.
13. G. W. WEBBER, W. R. BITLER and V. S. STUBICAN, *J. Phys. Chem. Solids* **41** (1980) 1355.
14. M. M. ABRAHAM, W. P. UNRUH and Y. CHEN, *Phys. Rev.* **B10** (1974) 3540.
15. M. M. ABRAHAM, Y. CHEN, L. A. BOATNER and R. W. REYNOLDS, *Phys. Rev. Lett.* **37** (1976) 849.
16. Y. CHEN, H. T. TOHVER, J. NARAYAN and M. M. ABRAHAM, *Phys. Rev.* **B16** (1977) 5535.
17. W. D. KINGERY, *J. Amer. Ceram. Soc.* **57** (1974) 1.
18. *Idem, ibid.* **57** (1974) 74.
19. W. C. JOHNSON, D. F. STEIN and R. W. RICE, in "Grain Boundaries in Engineering Materials", edited by J. L. Walter, J. H. Westbrook and D. A. Woodford (Claitors, Baton Rouge, La., 1975).
20. W. D. KINGERY, T. MITAMURA, J. B. VANDER SANDE and E. L. HALL, *J. Mater. Sci.* **14** (1979) 1766.

21. T. MITAMURA, E. L. HALL, W. D. KINGERY and J. B. VANDER SANDE, *Ceramurgia Int.* **5** (1979) 131.
22. J. R. BLACK and W. D. KINGERY, *J. Amer. Ceram. Soc.* **62** (1979) 176.
23. P. WYNBLATT and R. C. McCUNE, Proceedings of the Berkeley Conference on "Surface and Interfaces in Ceramics and Ceramic–Metal Systems" (Plenum, New York, 1981).
24. A. CIMINO, G. MINELLI and B. A. De ANGLIS, *J. Electron Spec. Related Phen.* **13** (1978) 291.
25. C. BERTHELET, W. D. KINGERY and J. B. VANDER SANDE, *Ceramurgia Int.* **2** (1976) 62.
26. W. D. KINGERY, W. L. ROBBINS, A. F. HENRIKSEN and C. E. JOHNSON, *J. Amer. Ceram. Soc.* **59** (1976) 239.
27. R. F. STEWART and W. C. MACKRODT, *J. Physique* **C7** (1976) 247.
28. W. C. MACKRODT and R. F. STEWART, *J. Phys.* **C10** (1977) 1431.
29. *Idem, ibid.* **C12** (1979) 431.
30. *Idem, ibid.* **C12** (1979) 5015.
31. W. C. MACKRODT, in "Atomic Transport in Solids", edited by F. Bénière and C. R. A. Catlow, Nato Advanced Study Institutes Series (Plenum, New York, 1982).
32. C. R. A. CATLOW, M. DIXON and W. C. MACKRODT, in "Computer Simulation of Solids", edited by C. R. A. Catlow and W. C. Mackrodt (Springer-Verlag, Berlin, 1982).
33. B. G. DICK and A. W. OVERHAUSER, *Phys. Rev.* **112** (1958) 90.
34. R. G. GORDON and Y. S. KIM, *J. Chem. Phys.* **56** (1972) 3122.
35. Y. S. KIM and R. G. GORDON, *ibid.* **60** (1974) 1842.
36. *Idem, ibid.* **60** (1974) 4332.
37. *Idem, Phys. Rev.* **B9** (1974) 3548.
38. A. I. M. RAE, *Chem. Phys. Lett.* **18** (1973) 574.
39. E. A. COLBOURN, J. KENDRICK and W. C. MACKRODT, ICI Corporate Laboratory Report CL-R/81/1637/A (1981).
40. K. K. KIM and A. S. NOWICK, *J. Phys.* **C10** (1979) 509.
41. C. R. A. CATLOW and R. JAMES, *ibid.* **C10** (1977) L237.
42. E. A. COLBOURN, J. KENDRICK and W. C. MACKRODT, unpublished results.
43. G. V. SAMSONOV, "The Oxide Handbook" (IFI/Plenum, 1973).
44. E. A. COLBOURN, W. C. MACKRODT and P. W. TASKER, unpublished results.
45. M. J. L. SANGSTER and A. M. STONEHAM, *Phil. Mag.* **B43** (1981) 597.
46. A. M. STONEHAM and M. J. L. SANGSTER, *ibid.* **B43** (1981) 609.
47. T. C. WADDINGTON, *Adv. Inorg. Chem. Radiochem.* **1** (1959) 157.
48. F. BASOLO and R. G. PEARSON, in "Mechanisms of Inorganic Reactions", 2nd edn. (Wiley, 1967).
49. P. GEORGE and D. S. McCLURE, *Prog. Inorg. Chem.* **1** (1959) 381.
50. C. R. A. CATLOW, I. D. FAUX and M. J. NORGETT, *J. Phys.* **C9** (1976) 419.
51. G. J. DIENES, D. O. WELCH, C. R. FISCHER, R. D. HATCHER, O. LAZARETH and M. SANDBERG, *Phys. Rev.* **B11** (1975) 3060.
52. R. C. WEAST (ed.) "C.R.C. Handbook of Physics and Chemistry" (C.R.C. Press, Boca Raton, 1981).
53. E. A. COLBOURN and W. C. MACKRODT, *Solid Stat. Commun.* **40** (1981) 265.
54. C. R. A. CATLOW, R. JAMES, W. C. MACKRODT and R. F. STEWART, *Phys. Rev.* **B25** (1982) 1006.

Received 2 March
and accepted 22 March 1982